IEEE Access
Multidisciplinary | Rapid Review | Open Access Journal

Received 6 January 2023, accepted 25 February 2023, date of publication 6 March 2023, date of current version 15 March 2023.

Digital Object Identifier 10.1109/ACCESS.2023.3252906

RESEARCH ARTICLE

Radially Extended 3D Birdcage Antenna for MRI With Loop-Type Legs and Connection to the Shield

CHAN-SUN PARK[1], DENIS TIHON[1], (Member, IEEE), FARZAD JABBARIGARGARI[1], REDHA ABDEDDAIM[2], AND CHRISTOPHE CRAEYE[1], (Senior Member, IEEE)

[1]Institute of Information and Communication Technologies, Electronics and Applied Mathematics (ICTEAM), Université Catholique de Louvain, 1348 Ottignies-Louvain-la-Neuve, Belgium
[2]Aix Marseille Univ, CNRS, Centrale Marseille, Institut Fresnel, Institut Marseille Imaging, 13013 Marseille, France

Corresponding author: Chan-Sun Park (chan-sun.park@uclouvain.be)

This work was supported in part by the European Commission through the M-Cube Project under Grant 736937, in part by the M-One Project under Grant 952106, and in part by the Excellence Initiative of Aix-Marseille University—A*MIDEX, a French ''Investissements d'Avenir'' Program through the Multiwave Chair of Medical Imaging.

ABSTRACT A novel radially extended 3D birdcage (BC) coil antenna was designed, simulated, and optimized for a cylindrical dielectric phantom at 4.7 T. The 3D birdcage consists of a classical birdcage with additional protrusions toward the inside and connections to the shield. To overcome the huge computational burden of the optimization process using the particle swarm optimization (PSO) method, an in-house method of moment (MoM) code exploiting the symmetry of the structure has been developed. The code produces open-circuit embedded element patterns and makes use of a Schur complement to analyze the effects of passive loads, in the presence of a phantom. The simulation results have been verified with the use of commercial software. The proposed 3D BC coil showed a 34 % improvement in the homogeneity of B_1^+ and a 37 % reduction in the peak specific absorption rate (SAR), compared with a conventional BC coil.

INDEX TERMS Birdcage antenna, birdcage coil, high-field magnetic resonance imaging, method of moments.

I. INTRODUCTION

Since the concept of magnetic resonance imaging (MRI) was first introduced to academia in the 1970s, MRI has been one of the key technologies for obtaining human or animal body images in vivo [1], [2], [3], [4]. The MRI machine generates images when protons in a molecule repeatedly absorb and relax energy from and to a radio frequency (RF) field when embedded in a static magnetic field B_0. In general, the RF magnetic field looked for, denoted as $B_1^+ = B_x + jB_y$, is circularly polarized and transverse to B_0. Continuous research has been carried out on the main components of MRI, such as main magnets and RF coils, as well as devices that control them [5].

Over the last few decades, many research programs aimed at improving the MRI systems in terms of homogeneity of the RF field magnitude, which translates into a homogeneous signal-to-noise ratio (SNR) in the image. In this endeavour, RF coils have gained more attention since they could be used in both transmitting and receiving modes. Although different types of volume coils have been introduced to improve the performance of the MRI system [6], [7], [8], the birdcage (BC) coil that was proposed by Hayes et al. [9] is still in wide use since it can produce a very homogeneous field over a wide volume. The conventional BC coil structure covered in this paper consists of two endrings at the top and bottom and multiple legs connecting them, as shown in Fig. 1. This coil showed significant performance improvement not only in terms of RF homogeneity but also in terms of the SNR. Ideally, if a BC coil stretches out infinitely along the longitudinal axis and has a number of legs that tends toward infinity, an almost perfectly homogeneous transverse magnetic field can be produced by a surface current flowing along the axial direction of the cylinder with an amplitude

The associate editor coordinating the review of this manuscript and approving it for publication was Jinhua Sheng.

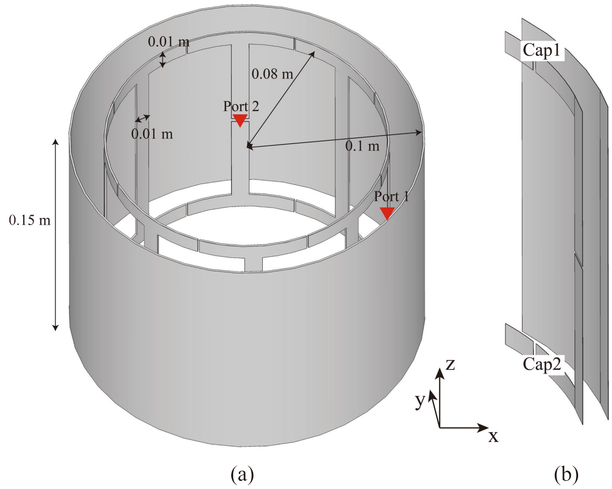

FIGURE 1. (a) Scheme of the conventional birdcage coil used as a reference. (b) detailed view of one of the sectors of the BC coil.

varying as $\sin\theta$, where θ is the azimuthal angle [10, Chapter 8]. In practice, the magnitude of the current flowing through each of N legs can be controlled to a large part by adjusting the capacitance values inserted into the endrings or legs [11], which makes it possible to create a highly homogeneous field inside the coil. A birdcage coil supports $N/2+1$ resonances. One is formed by end ring current loops. The other ones correspond to closed current loops involving both the legs and end rings. The resonant mode used in MRI is the dominant mode. It forms a sinusoidal current magnitude on the legs, resulting in a homogeneous field inside the volume of the coil.

In order to obtain better quality images, MRI machines have gradually used higher magnetic fields such as 3 T, 4.7 T, and 7 T. The Larmor frequency being proportional to B_0, the RF operating frequency has increased accordingly. However, the conventional BC coil was ideally operated under the condition that the RF frequency was below the cut-off frequency of the MRI tunnel (or shield), even when loaded by the human body. This condition is no longer satisfied at the higher RF frequencies currently considered. It deteriorates the homogeneity when higher B_0 fields are used, as a standing wave appears in the MRI tunnel [12], [13], [14], [15], [16], [17].

In order to obtain a more homogeneous RF field and to get more accurate clinical images, several research projects aimed at tailoring the RF field interference effects by exploiting a passive shimming [18] (such as the use of high-permittivity dielectric materials [19]) or by using an active shimming (such as transmit arrays or pTx [20]).

In this paper, we introduce a novel BC coil with improved performance by modifying the structure of the coil, which can be categorized as a new shimming technique. This modification consists of a tight transmission-line inspired link between the coil and the shield and of extra legs placed on an inner ring. Two main figures of merit (FoMs) regarding RF fields in MRI, field homogeneity and specific absorption rate (SAR), are taken as the criteria of coil performance. The

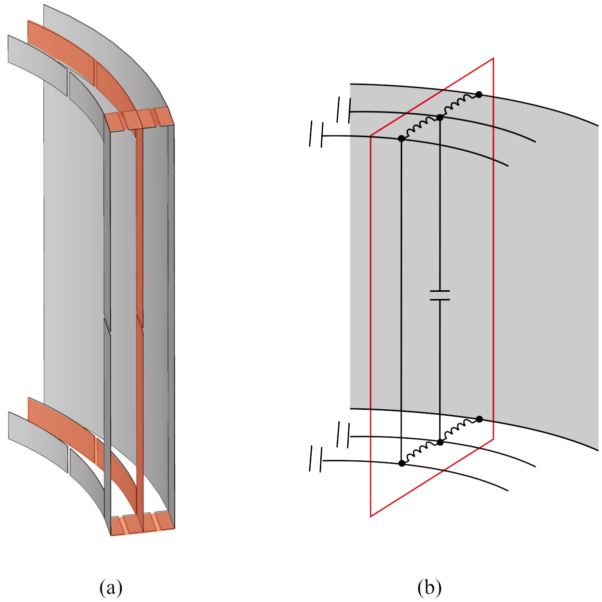

FIGURE 2. (a) Geometry and (b) electrical scheme of a sector of the proposed volumetric BC coil.

homogeneity of B_1^+ of the coil is more important than the radiation efficiency because it is not a structure intended to radiate the field to a far location as in typical antennas; also, the maximum SAR is more crucial than the radiation pattern of the coil. Field inhomogeneity, already mentioned above, causes a direct decline in image quality, such as shading, spatial distortion, blurring [21], and intensity loss; therefore, field homogeneity is essential for the MRI coil. SAR is a quantity related to the safety aspects of MRI, which is defined as the power per unit mass absorbed by tissues when exposed to the RF field; it is given by

$$SAR = \frac{\sigma |E|^2}{2\rho}, \tag{1}$$

where σ and ρ are the conductivity and the mass density of the tissue respectively and $|E|$ is the magnitude of the electric field in the tissue. Local and global limitations on SAR are usually applied in order to avoid damaging tissues through local or global elevation of the temperature.

This paper is organized as follows. In Section II, solutions to the homogeneity problem are reviewed and the proposed BC coil structure is introduced. Section III describes the numerical method devised to efficiently analyze and optimize the coil. The performance of the improved BC coil is shown in Section IV. Conclusions are drawn in Section V.

II. GEOMETRY OF THE PROPOSED BIRDCAGE COIL

Obtaining homogeneous B_1 fields and low SAR values is always a challenging research topic in the MRI area. The birdcage antenna has shown quite effective performance in the medical imaging field, but better performance is still required as B_0 goes higher. Also the presence of the shielding cylinder may cause low antenna impedance and may also exacerbate the above-mentioned inhomogeneity. Several authors [22], [23], [24], [25], [26], [27], [28] tried to create high-impedance surfaces on the shield, for instance using mushroom-type particles, and could achieve improved transmit efficiency for the MRI coil. As an alternative to high-impedance surfaces, we propose a volumetric approach, in which the birdcage is physically connected to the shield, using a number of series and parallel strips (respectively in the radial and axial directions), each of which is terminated with a reactive load (inductor or capacitor) as in Fig. 2.(a).

Several papers and patents have already proposed different types of connection between a shield and a leg. In [29], legs are cut in the middle and connected to the shield in order to be able to insert another instrument in the MRI tunnel. In [30], a radial strip connects the legs to a ring located between the birdcage and shield in order to tune the operating frequency. The transverse electromagnetic (TEM) resonator coil [8], [17], [31], [32], which is a structure that has a direct connection between the leg and the shield, is one of the most widely used MRI coils along with the BC coil; it is distinguished from the BC coil because there is no endring connecting the legs.

The difference between the BC coil proposed in this paper and the aforementioned studies lies in the presence of radial inductively loaded connections between the BC and the shield and additional axial capacitively loaded legs, as illustrated in Fig. 2(b). The additional structure mimics the ladder model of a transmission line and acts as an "impedance bridge". The phase velocity in that transmission line commands the rate at which impedance changes along the line (from very low on the shield to high at the level of the birdcage antenna), while the characteristic impedance impacts the antenna matching. This is obtained through proper positioning of the additional conducting strips and through a joint optimization of the capacitance and inductance values in the structure.

III. NUMERICAL METHODS USED FOR ANALYSIS AND OPTIMIZATION

As mentioned in Section II, a proper optimization of the value of the capacitors and inductors is essential to obtain good performances, *i.e.* low SAR peaks, homogeneous B_1^+ field and good impedance matching of the input ports in the presence of a sample that is being imaged. The optimization algorithm focused on the generation of homogeneous B_1^+ field in the central transverse plane of the phantom. Indeed, a homogeneous B_1^+ field on that plane is associated with an optimal current distribution on the BC coil. Such an optimal current distribution also exhibits a large field of view in the axial direction and low SAR peaks, as will be shown in Section IV. As for the matching, it is implicitly realized by favoring high field intensity in the evolutionary algorithm used for optimization; this prevents the solution from being affected by a too-large reflection loss between the generator and birdcage.

Optimum values for the lumped elements have been found using the particle swarm optimization (PSO) [33] method. First, a cost function is defined. To any set of lumped element values, it associates a real number that describes the "quality" of the corresponding antenna. In our case, the quality criterion is formulated in terms of field homogeneity. The impedance matching of the coil is implicitly guaranteed by the convergence criterion of the PSO, which ensures a good field intensity in the center of the coil. In our case, we define the cost function as the normalized standard deviation ($\mathtt{NSD}$) of the B_1^+ field, formulated as

$$\mathtt{NSD}(B_1^+) = \frac{\mathtt{Std}(B_1^+)}{\mathtt{Mean}(B_1^+)}, \tag{2}$$

where

$$\mathtt{Mean}(B_1^+) = \frac{\iint |B_1^+(\mathbf{r})| d\mathbf{r}}{S}, \tag{3}$$

$$\mathtt{Std}(B_1^+) = \sqrt{\frac{\iint (|B_1^+(\mathbf{r})| - \mathtt{Mean}(B_1^+))^2 d\mathbf{r}}{S}}, \tag{4}$$

and S is the area of the transverse section of the phantom.

Once the cost function is defined, a set of candidate solutions is generated randomly and simulated. The cost function associated with each solution of the set is estimated, providing a measure of their quality. To improve the quality of the candidate solutions, the PSO algorithm treats each solution as a particle moving in the solution-space, *i.e.* a M-dimensional space, M corresponding to the number of lumped elements. At each iteration, each particle's movement is affected by its local best-known position, but it is also guided toward the best-known positions in the whole solution-space, as found by the other particles. This leads the swarm of particles to move toward the optimum solutions.

Since for each candidate solution, a full simulation of the BC coil is needed, an in-house software based on the Method of Moments (MoM) was used to accelerate the procedure. The code was optimized to minimize the computation time required to obtain the cost function for many different sets of loads when the geometry of the BC coil is fixed. The main features of the geometry are:

- the presence of perfectly electrically conducting (PEC) sheets to model the birdcage, the shielding and the impedance bridges,
- the presence of lumped electrical elements (capacitors, inductors and ports) whose values need to be optimized,
- the presence of a lossy dielectric cylinder used as a phantom,
- an 8-fold rotational symmetry that is only broken by the ports and that can be exploited to accelerate the computations.

A. THE METHOD OF MOMENTS

The Method of Moments solves Maxwell's equations in surface integral form and can deal with piecewise homogeneous

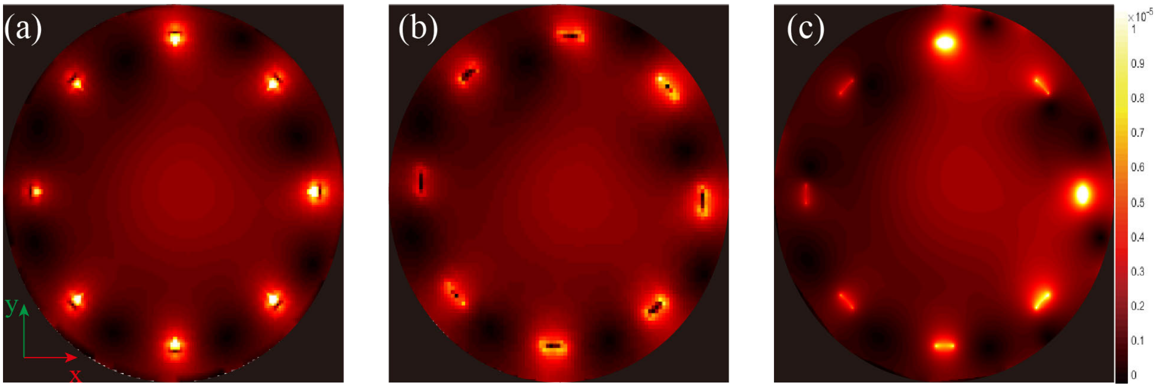

FIGURE 3. B_1^+ **field from (a) in-house MoM (b) CST and (c) FEKO.**

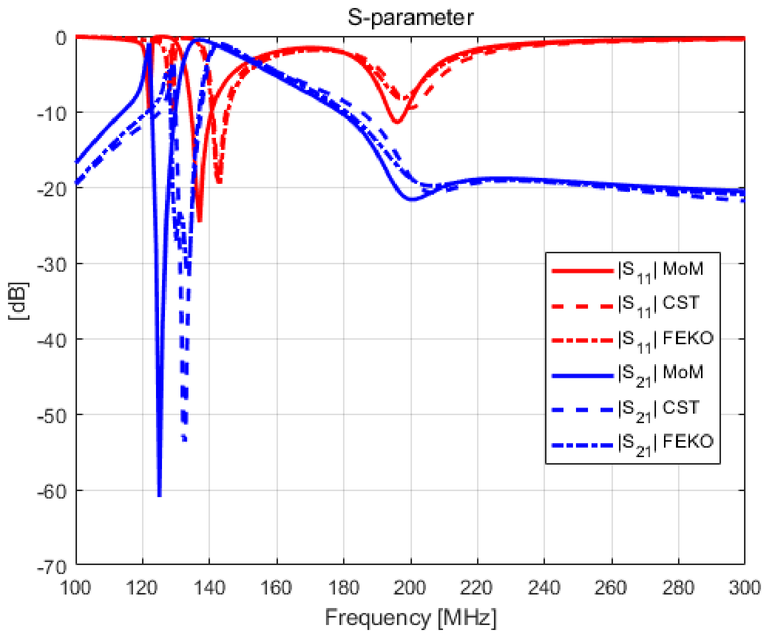

FIGURE 4. S-parameter analysis of the conventional BC coil using the in-house MoM, CST and FEKO.

geometries through the use of the equivalence principle [34], [35], [36], [37].

The unknown equivalent currents used to mimic the response of the structure are found by imposing boundary conditions [38]. For PEC surfaces, it corresponds to a vanishing electric field. For penetrable bodies, it corresponds to the continuity of the tangential electric and magnetic fields across the interface.

To study the field generated by the BC coil, the metallic surface of the antenna (shield, BC coil, and impedance bridges) and the surface of the dielectric phantom are discretized using a set of basis and testing functions. The basis functions are used to approximate the equivalent currents on the different surfaces. The testing functions are used to impose the boundary conditions on the different interfaces. In order to model the lumped elements (ports, capacitors and inductors), a delta-gap model is used [39]. The lumped elements are modeled using basis functions that bridge the infinitesimal gap separating different conductive parts of the geometry. The current flowing along these basis functions depends on the voltage that builds up across the gap and the impedance of the lumped elements. Imposing the boundary conditions across the conducting surfaces and the dielectric interface and imposing the I-V relation across the lumped elements, one has to solve the following system of equations

$$\begin{pmatrix} Z_{cc} & Z_{cd} & Z_{cp} \\ Z_{dc} & Z_{dd} & Z_{dp} \\ Z_{pc} & Z_{pd} & Z_{pp}^{\text{tot}} \end{pmatrix} \cdot \begin{pmatrix} \mathbf{x}_c \\ \mathbf{x}_d \\ \mathbf{x}_p \end{pmatrix} = \begin{pmatrix} \mathbf{0} \\ \mathbf{0} \\ -\mathbf{b}_p \end{pmatrix}, \tag{5}$$

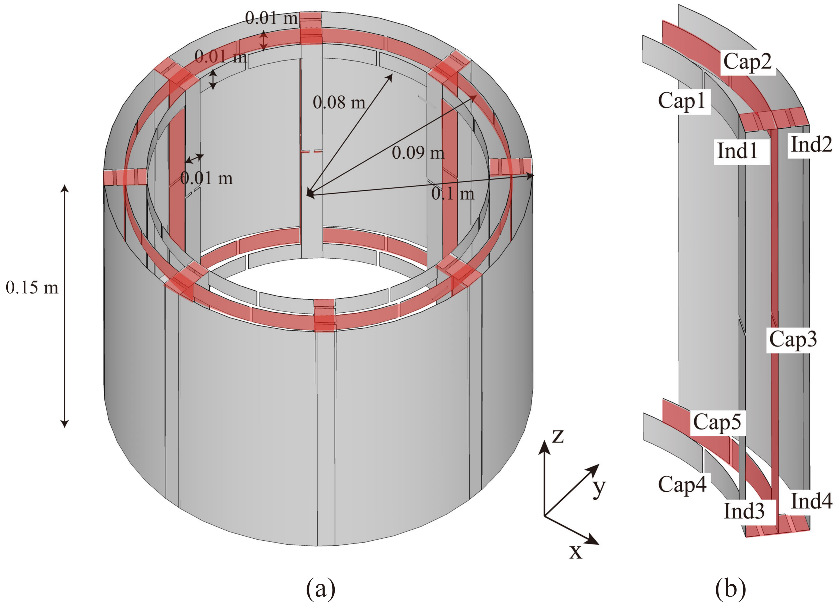

FIGURE 5. (a) Geometry of the proposed BC coil #1. (b) Detailed view of one sector of the BC coil. The novel features of the proposed design (*i.e.* the impedance bridges) have been highlighted.

with c, d and p subscripts corresponding to the PEC surfaces, dielectric interface and port basis and testing functions. Entry (i, j) of Z_{lm} describes the interactions between the jth basis function of surface m and the ith testing function of surface l. $\mathbf{x}_l$ is the unknowns vector whose ith entry corresponds to the amplitude of the currents along the ith basis function of surface l. $\mathbf{b}_p$ is a vector that describes the excitation of the ports of the antenna. The Z_{pp}^{tot} matrix corresponds to the classical MoM impedance matrix Z_{pp} except for the self-interaction terms, for which the contribution of the lumped element is added. The self-interaction term of lumped element i whose impedance is Z_i reads

$$Z_{pp}^{\text{tot}}[i, i] = Z_{pp}[i, i] - Z_i w^2 \tag{6}$$

with w the width of the basis function at the position of the gap and $Z[i, j]$ the (i, j) entry of matrix Z. Similarly, if a port i is excited with a voltage amplitude V_{exc}, the corresponding entry of the excitation vector $\mathbf{b}_p$ becomes

$$\mathbf{b}_p[i] = -V_{\text{exc}} w. \tag{7}$$

It can be noticed that only a tiny portion of the total impedance matrix changes when the value of the lumped elements is modified. Thus, using the Schur complement, one can invert the part of the impedance matrix that does not vary and use the result for every different set of loads, leading to the reduced system of equations

$$\tilde{Z}_{pp}^{\text{tot}} \cdot \mathbf{x}_p = -\mathbf{b}_p \tag{8}$$

with

$$\tilde{Z}_{pp}^{\text{tot}} = Z_{pp}^{\text{tot}} - \begin{pmatrix} Z_{pc} & Z_{pd} \end{pmatrix} \cdot \begin{pmatrix} Z_{cc} & Z_{cd} \\ Z_{dc} & Z_{dd} \end{pmatrix}^{-1} \cdot \begin{pmatrix} Z_{cp} \\ Z_{dp} \end{pmatrix} \tag{9}$$

Algorithm 1 Algorithm Used to Optimize the Lumped Elements Value of a Given BC Coil Geometry

Compute Z_{cc}, Z_{cd}, Z_{cp}, Z_{dc}, Z_{dd}, Z_{dp}, Z_{pc}, Z_{pd}, Z_{pp} and Z_{td}
Evaluate $\tilde{Z}_{pp}$ for short-circuited elements using (9)
Compute Z_{tp}^{oc} using (11)
Generate a set of 1000 candidate solutions
while Solution can be improved **do**
  for Candidate solution in the set **do**
    Update $\tilde{Z}_{pp}$ using (6)
    Find $\mathbf{x}_p$ solving (8)
    Compute B_1^+ field using (10)
    Evaluate $\mathtt{NSD}(B_1^+)$ using (2), (3) and (4)
  end for
  Update the set of candidate solutions using PSO
end while

The solution of (9) has been accelerated using the block-circulant nature of the Z_{cc}, Z_{cd}, Z_{dc} and Z_{dd} matrices [40], [41], which is a consequence of the rotational symmetry of the corresponding geometrical entities.

Last, solving (8) only provides the currents $\mathbf{x}_p$ flowing across the lumped elements. To rapidly evaluate the cost function associated with these currents, the open-circuit (o.c.) embedded element pattern of each port is precomputed. Using the subscript t to designate the testing functions used to image the magnetic field inside the phantom, the value of the field along the testing functions reads

$$\mathbf{f}_t = Z_{tp}^{\text{oc}} \cdot \mathbf{x}_p \tag{10}$$

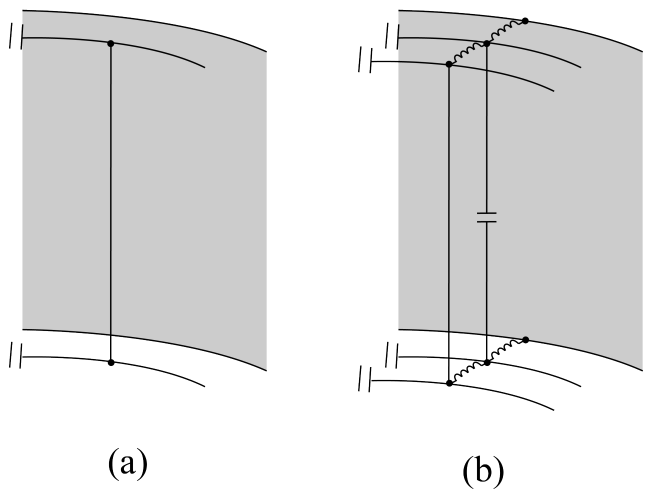

FIGURE 6. Electrical scheme of (a) conventional birdcage coil and (b) birdcage coil model #1.

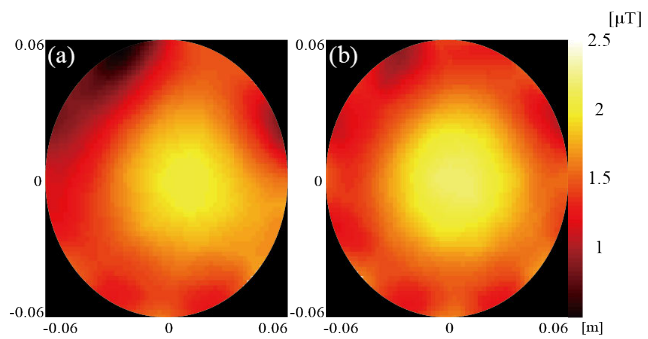

FIGURE 7. B_1^+ of (a) Conventional BC coil, NSD = 0.214 (b) Proposed 3D BC coil model #1, NSD = 0.171.

with

$$Z_{tp}^{oc} = \begin{pmatrix} 0_{tc} & -Z_{td} \end{pmatrix} \cdot \begin{pmatrix} Z_{cc} & Z_{cd} \\ Z_{dc} & Z_{dd} \end{pmatrix}^{-1} \cdot \begin{pmatrix} Z_{cp} \\ Z_{dp} \end{pmatrix} \tag{11}$$

with 0_{ij} a null matrix of the same size as Z_{ij}. The minus sign of (11) comes from the fact that, using the equivalence principle, the currents inside and outside the phantom have opposite sign [34]. It can be noticed that Z_{tp}^{oc} does not depend on the value of the lumped elements and can thus be computed once and stored for subsequent uses.

The algorithm used to exploit the acceleration techniques described in this section is visible in Algorithm 1. The time consumption of each step for a typical optimization procedure is the following. We consider a BC coil whose PEC surfaces and phantom are discretized using 5632 and 288 basis functions, respectively. The basis functions used to mesh the surface of the phantom were used to expand both the equivalent electric and magnetic surface currents, leading to 576 associated unknowns. Using the algorithm described in Algorithm 1, the value of the 56 lumped elements involved in the geometry was optimized. It took approximately 35 minutes to compute the impedance matrices (line 1 of Algorithm 1) and 36 additional seconds to evaluate $\tilde{Z}_{pp}$ and the embedded element patterns (lines 2 and 3). Once the preparation steps are finished, the computation of the cost function for a given candidate solution took approximately 9 ms (lines 7 to 10). The PSO required 14 iterations with a swarm of 1000 particles, leading to a total time of 124 seconds. As can be seen, the optimization time remains small compared to the preparation time, showing the effectiveness of the acceleration techniques used.

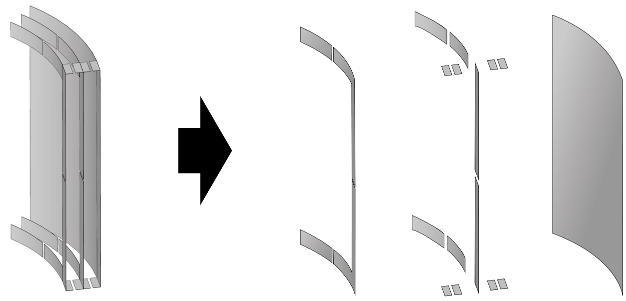

FIGURE 8. Separating supplemental elements of 3D BC coil by parts.

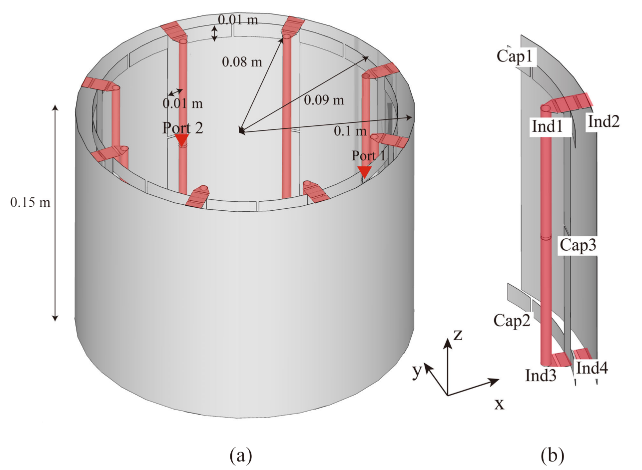

FIGURE 9. (a) Geometry of the BC coil model #2. (b) Detailed view of a sector.

IV. RESULTS

Before comparing the results, validation of the in-house MoM code has been carried out via comparison with simulation results obtained with the commercial software CST Microwave Studio and FEKO. The geometry used here is a conventional 4.7 T BC coil with a phantom and a conducting shield. The phantom used in this analysis has a 0.06 m radius and a 0.2 m height with a relative permittivity of 61 and a conductivity of 0.8 $\Omega^{-1}m^{-1}$, which reflect human tissue characteristics. Figs. 3 and 4 show the B_1^+ field for a frequency of 200 MHz and the S-parameter analysis for frequencies between 100 MHz and 300 MHz for the BC coil shown in Fig. 1. It is almost impossible to obtain exactly the same results when we use different types of numerical

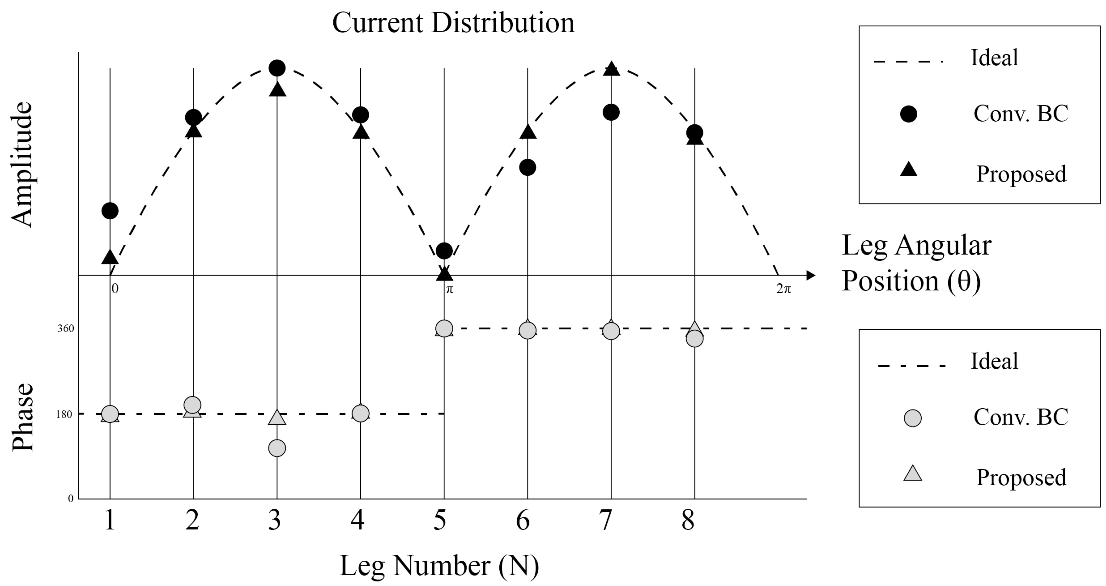

FIGURE 10. Current distribution on the legs of the ideal, conventional BC coil and proposed BC coil.

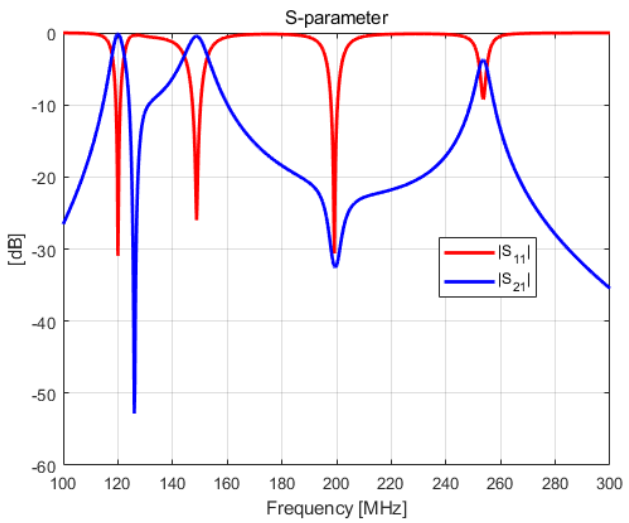

FIGURE 11. S-parameter of optimized proposed BC coil.

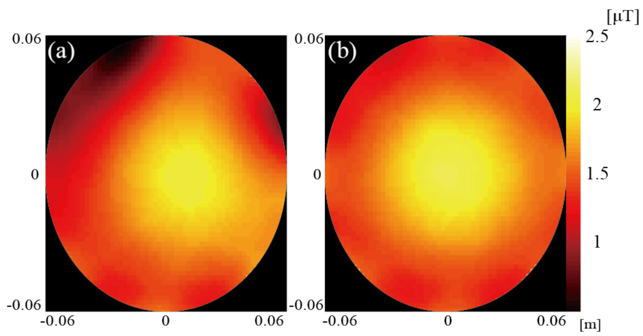

FIGURE 12. B_1^+ of (a) Conventional BC coil, NSD = 0.214 (b) Proposed 3D BC coil model #2, NSD = 0.14.

methods or solvers because formulations and mesh shapes are different between every numerical analysis technique. However, since the above results yield very similar results based on the field distribution and S-parameter among the three different analysis schemes, we think it is sufficient to verify the validity of the analysis technique. As can be seen in Figs. 3 and 4, the in-house MoM code shows a good agreement with the commercial software results.

A. FINAL DESIGN OF THE PROPOSED BC COIL

Figs. 1, 5 and 6 show the structure of the conventional BC coil, the initial model of the proposed 3D BC coil, and the layout of lumped elements included in that structure. Both the conventional BC coil and the proposed BC coil have 0.15 m height, conducting shield with 0.1 m radius and 0.08 m the innermost radius of coils. Detailed dimensions of the structures can be found in Fig. 5. The conventional BC coil consists of the top and bottom endrings, the legs connecting them, and the conducting shield surrounding both. The initial model of the proposed 3D BC coil corresponds to the conventional BC coil with additional transmission line-type impedance bridges. The latter are made of additional endrings connected by legs and radial strips connecting the BC to the shield. The supplemental elements are highlighted in Fig. 5. Both structures are excited with two ports with a 90° phase-shift in order to selectively excite the mode that is rotating in the "appropriate" direction. Through the numerical analysis and optimization method described in Section III, the optimized lumped inductance and capacitance values inserted into the structure were obtained. This procedure led to a new type of 3D BC coil.

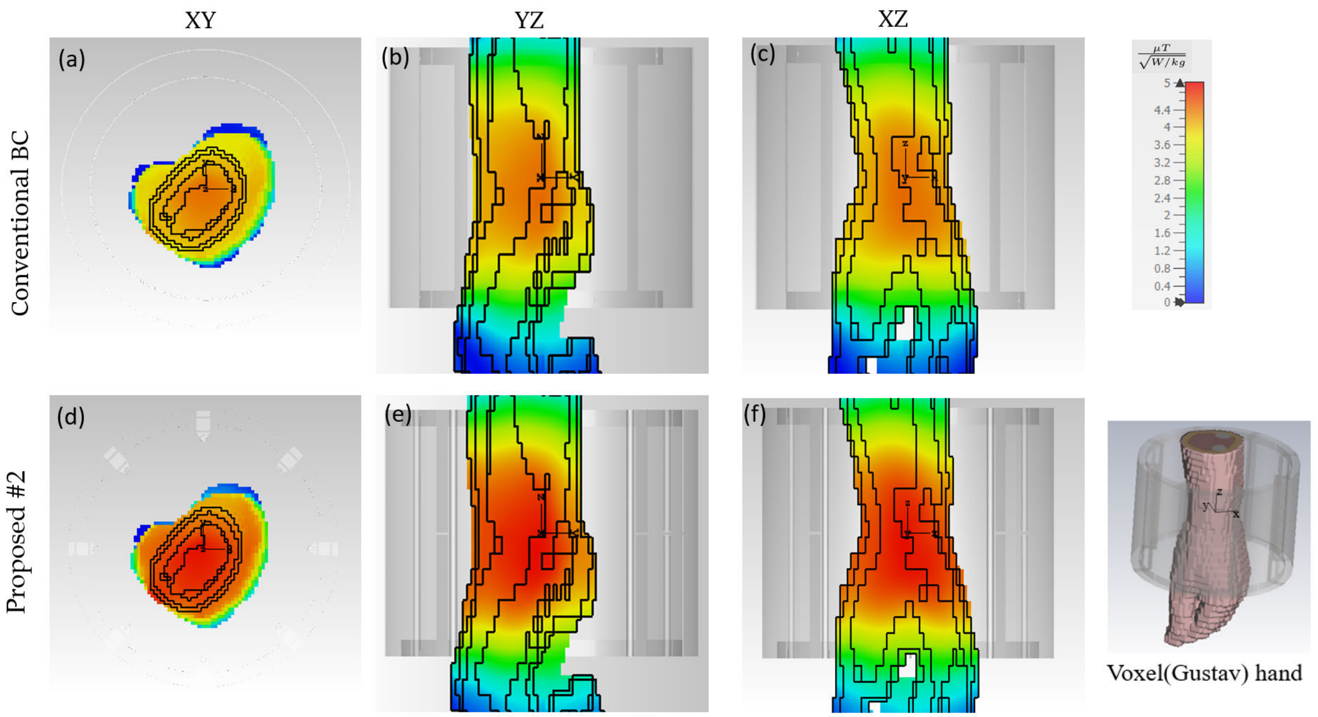

FIGURE 13. $\frac{B_1^+}{\sqrt{SAR_{max}}}$ for 1 W accepted power for (a)-(c) Conventional BC (d)-(f) model #2 in voxel wrist (Gustav).

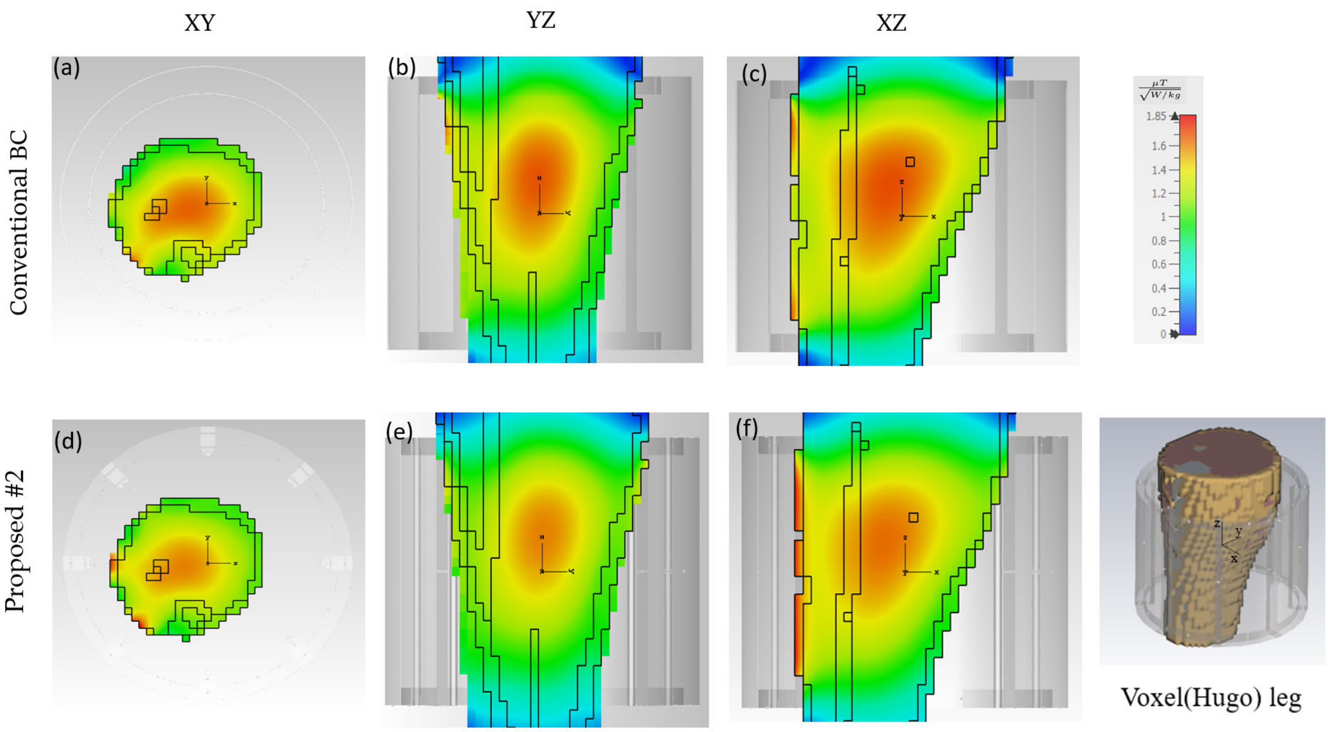

FIGURE 14. $\frac{B_1^+}{\sqrt{SAR_{max}}}$ for 1 W accepted power for (a)-(c) Conventional BC (d)-(f) model #2 in voxel leg (Hugo).

When looking at the NSD, which is the quantitative measure of field uniformity mentioned earlier in equation (2), the first model of the proposed BC coil has an NSD of 0.171, which is significantly improved with respect to

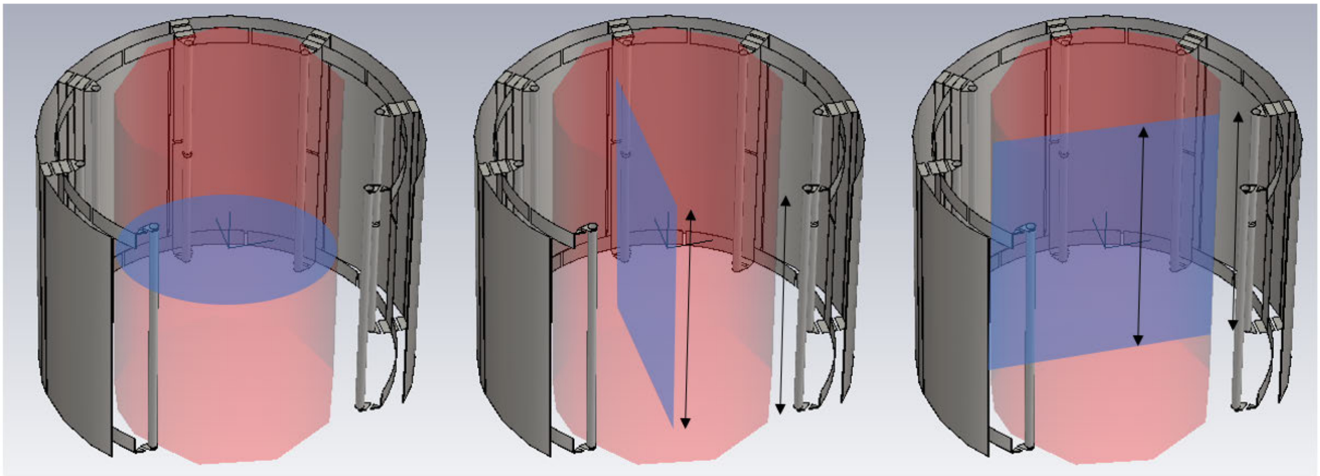

FIGURE 15. Exact location of each plane in Fig. 16. (a) XY plane (b) YZ plane (c) XZ plane.

TABLE 1. Values of the optimized loads in the BC coil model #2.

Cap1 / Cap2	4.08 pF
Cap3	0.355 pF
Ind1 / Ind3	0.086 uH
Ind2 / Ind4	0.203 uH

the conventional BC coil (NSD = 0.214), as shown in Fig. 7.

Although the first proposed BC coil with optimized lumped elements values showed superior performance compared to the conventional BC coil, the resulting field was not entirely symmetric in the azimuthal direction.

To further improve the design, we looked for redundancies within the degrees of freedom offered to the optimizer. A new design have been obtained using the following approach:

- Divide the supplemental parts in the initial 3D BC coil by each element. (as in Fig. 8.)
- Try several candidate structures in which the additional elements are arranged differently.
- Compare the performance of each structure to find the optimal one.

As a result, it was possible to obtain the most homogeneous and circularly symmetric B_1^+ field from the structure shown in Fig. 9. The detailed values of the optimized loads are in Table. 1. The NSD of the above structure is 0.14, which is about 22% better than the 0.171 of the model #1. The reason of this performance improvement can be seen by observing the magnitude and phase of the current induced in each leg, which is the main source that generates the field inside the birdcage coil.

As can be seen in Fig. 10, homogeneous fields come from the improved current distribution on the legs, which is closer to the ideal sinusoidal distribution [42].

In the case of the newly invented BC coil, an additional impedance matching has been successfully conducted by making use of the supplemental impedance bridges, as can be seen in Fig. 11, which results in the current distribution close to the ideal one, as in Fig. 10. As a result, it was possible to obtain a field distribution with circular symmetry and a much more homogeneous field than the field of the conventional BC coil.

This optimum structure eliminated redundant endrings (shown in Fig. 5), which were not included in the dominant resonance path, and maintained the essential impedance bridges that can perform the impedance matching. It yielded further improved results, as shown in Fig. 12. Besides, special care has been taken to keep the innermost radius of the coil at a constant value, to avoid shrinking of the actual observation area.

In addition, in order to further check the reliability and efficiency of the newly proposed design, simulations were performed on the wrist and calf of the human body using a mesh file that provides the human body model in voxel form, and the analysis was conducted. As for the voxel model used, among the models provided by CST [43], model "Gustav" was used for the wrist, and model "Hugo" was used for the calf. The results are as follows.

For this example, the homogeneity was judged using a simplified homogeneity metrics (SHM) due to the difficulty to extract and integrate fields from the complex model. The simplified homogeneity index is obtained from the normalized extremum fields to the maximum values of SAR and corresponds to $(\frac{B_{1\ max}^+}{\sqrt{SAR_{max}}} - \frac{B_{1\ min}^+}{\sqrt{SAR_{max}}})$ divided by $(\frac{B_{1\ max}^+}{\sqrt{SAR_{max}}} + \frac{B_{1\ min}^+}{\sqrt{SAR_{max}}})/2$.

As shown in Fig. 13, and in Fig. 14, and the SHM values in Table. 2, the proposed structure shows better homogeneity indices in both the wrist and calf.

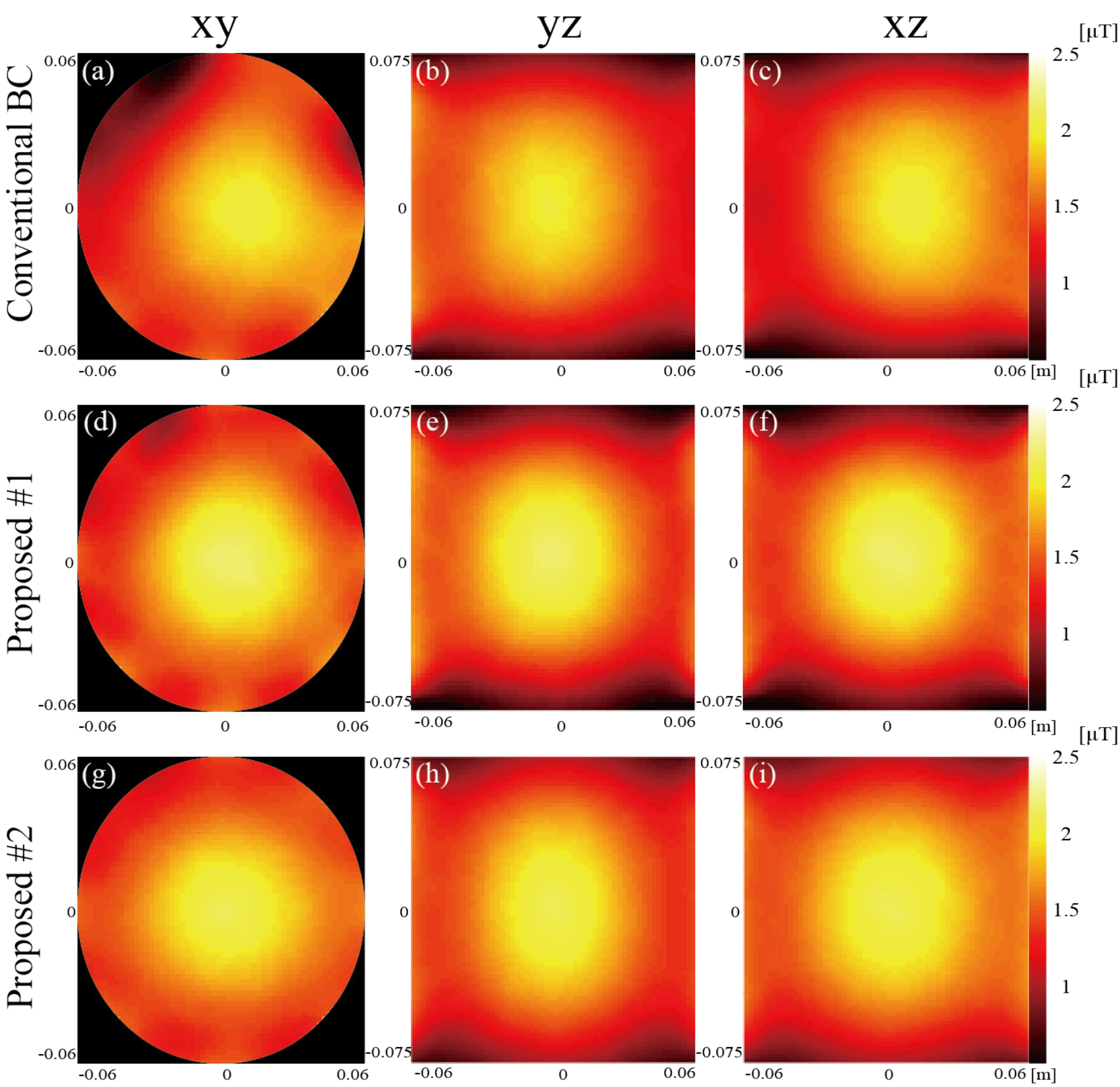

FIGURE 16. Volumic B_1^+ of (a)-(c) Conventional BC (d)-(f) model #1 (g)-(i) model #2.

TABLE 2. Maximum, minimum B_1^+ and simplified homogeneity index in the voxel models.

Body organ	$\frac{B_1^+{}_{max}}{\sqrt{SAR_{max}}}$	$\frac{B_1^+{}_{min}}{\sqrt{SAR_{max}}}$	SHM
Wrist - conventional BC	4.4	1.5	0.98
Wrist - proposed BC	4.95	2.2	0.76
Calf - conventional BC	1.33	0.22	1.43
Calf - proposed BC	1.85	0.6	1.02

TABLE 3. Stability analysis of the proposed BC coil for different radius phantoms (0.055, 0.06(defalut), 0.065 and 0.07 m).

Phantom radius	Resonance frequency deviation	NSD
0.055 m	+0.7 MHz	0.143
0.06 m (Default)	-	0.14
0.065 m	+0 MHz	0.142
0.07 m	+0.1 MHz	0.14

B. EXTENSIVE VALIDATION OF THE FINAL DESIGN

Due to the characteristics of MRI, it is necessary to look at the other parameters, such as the entire field in the volume of interest, the SAR, and the robustness of the results. Fig. 15 shows the XY, YZ, and XZ cross-sections, and Fig. 16 provides the corresponding field

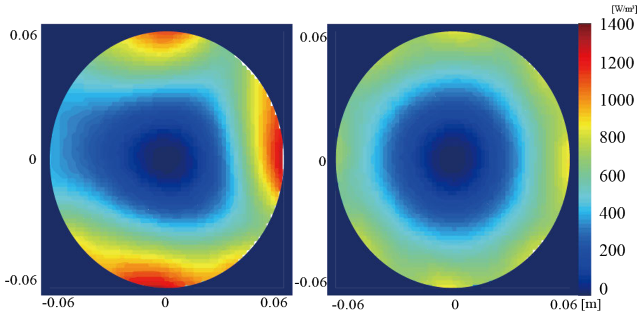

FIGURE 17. SAR distribution of (a) Conventional BC coil, peak SAR = 1410 [W/m^3] (b) Proposed 3D BC coil model #2, peak SAR = 896[W/m^3].

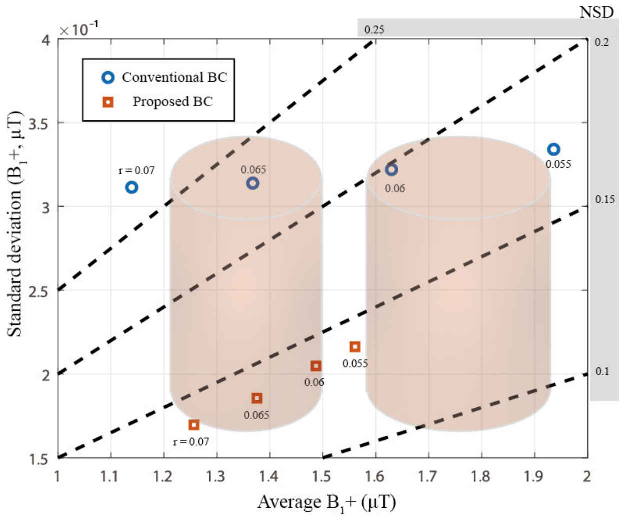

FIGURE 18. BC coil performance with different phantom radii.

distributions on these cuts for the three coils we analyzed earlier.

The field generated by the conventional BC is skewed in the XY, YZ, and XZ planes, exhibiting poor uniformity. In the case of model #1 of the 3D BC coil, a better spatial uniformity is obtained, as compared to the conventional birdcage. However, model #2, offers a slightly larger field of view. Since the current distribution induced in each leg in model #2 is most similar to the current distribution of the ideally designed BC coil, it can be confirmed that a homogeneous B_1^+ field is formed in the widest area inside.

In addition to the field homogeneity, the proposed birdcage coil also has strengths from the viewpoint of the peak SAR, which is one of the most important FoMs of the MRI coil. As can be seen in Fig. 12, the field of the proposed birdcage coil is distributed as uniformly as possible in the region of interest. Therefore the SAR spreads evenly over the entire area rather than showing a specific peak value, thus reducing the heat on the tissues and minimizing the risk. It can be seen from Fig. 17 that the peak SAR of the proposed BC coil is 896 W/m^3, i.e., very small compared to the one obtained with the conventional BC coil which was 1410 W/m^3.

Finally, we examined the stability of the performances for a fixed set of loads for varying sizes of the phantom. The phantoms with different radii of 0.055, 0.06 (default), 0.065, and 0.07 m were placed into the same proposed coil, and the resonant frequencies and NSD were computed. The results are provided in Table 3. Over the whole range of phantom sizes that have been investigated, a maximum frequency shift of 0.7 MHz and a maximum variation of the NSD of 2.1% was observed, confirming the robustness of the design. Also, the stability of both the conventional BC coil and the proposed coil are plotted in Fig. 18. It can be confirmed that the NSD of the proposed BC coil remains stable when the radius of the phantom varies, while the NSD of the conventional BC coil changes considerably. As monitored from MoM simulations, from a fabrication point of view, the optimized value of the lumped elements can be chosen with a tolerance of 2%, corresponding to a frequency shift between 1 and 2 MHz, which can be corrected with a standard tuning circuit.

V. CONCLUSION

A high-frequency birdcage coil producing a very homogeneous B_1^+ field and low SAR peaks has been described. The design makes use of connections between the BC and the shield that mimics the ladder model of a transmission line. The loads involved in the design have been optimized using an in-house MoM code combined with PSO optimization. The conventional BC coil and two proposed improved geometries have been analyzed and compared. With respect to the traditional BC coil geometry, the best design provides a 34% improvement in field homogeneity and a 37% reduction of peak SAR value. Good stability versus phantom size has also been observed. Given its high homogeneity, the new design is expected to provide a practically constant brightness (SNR) over a large field of view.

ACKNOWLEDGMENT

The authors would like to thank Constantine Simovski, Marc Dubois, Stanislav Glybovski, and Julien de Rosny for interesting discussions regarding birdcage antennas and high-impedance surfaces.

REFERENCES

[1] P. C. Lauterbur, "Image formation by induced local interactions: Examples employing nuclear magnetic resonance," *Nature*, vol. 242, pp. 190–191, Mar. 1973.

[2] P. Mansfield and A. A. Maudsley, "Medical imaging by NMR," *Brit. J. Radiol.*, vol. 50, no. 591, pp. 188–194, Mar. 1977.

[3] P. Mansfield, "Multi-planar image formation using NMR spin echoes," *J. Phys. C, Solid State Phys.*, vol. 10, no. 3, pp. L55–L58, Feb. 1977.

[4] P. Mansfield and P. G. Morris, *NMR Imaging in Biomedicine: Supplement 2 Advances in Magnetic Resonance*. London, U.K.: Academic, 1982.

[5] W. R. Hendee and E. R. Ritenour, *Medical Imaging Physics*. Hoboken, NJ, USA: Wiley, 2003.

[6] H. Hanssum, "The magnetic field of saddle-shaped coils. I. Symmetry of the magnetic field around the coil centre," *J. Phys. D, Appl. Phys.*, vol. 17, no. 1, p. 1, 1984.

[7] C. E. Hayes, N. Hattes, and P. B. Roemer, "Volume imaging with MR phased arrays," *Magn. Reson. Med.*, vol. 18, no. 2, pp. 309–319, Apr. 1991.

[8] J. T. Vaughan, H. P. Hetherington, J. O. Otu, J. W. Pan, and G. M. Pohost, "High frequency volume coils for clinical NMR imaging and spectroscopy," *Magn. Reson. Med.*, vol. 32, no. 2, pp. 206–218, 1994.

[9] C. E. Hayes, W. A. Edelstein, J. F. Schenck, O. M. Mueller, and M. Eash, "An efficient, highly homogeneous radiofrequency coil for whole-body NMR imaging at 1.5 T," *J. Magn. Reson.*, vol. 63, no. 3, pp. 622–628, Jul. 1985.

[10] J. Mispelter, M. Lupu, and A. Briguet, *NMR Probeheads for Biophysical and Biomedical Experiments: Theoretical Principles and Practical Guidelines*. Singapore: World Scientific, 2015.

[11] J. Jin, *Electromagnetic Analysis and Design in Magnetic Resonance Imaging*. Boca Raton, FL, USA: CRC Press, 1998.

[12] T. S. Ibrahim, R. Lee, B. A. Baertlein, Y. Yu, and P.-M.-L. Robitaille, "Computational analysis of the high pass birdcage resonator: Finite difference time domain simulations for high-field MRI," *Magn. Reson. Imag.*, vol. 18, no. 7, pp. 835–843, Sep. 2000.

[13] J. Chen, Z. Feng, and J.-M. Jin, "Numerical simulation of SAR and B_1-field inhomogeneity of shielded RF coils loaded with the human head," *IEEE Trans. Biomed. Eng.*, vol. 45, no. 5, pp. 650–659, May 1998.

[14] J. Chen and J. M. Jin, "Calculation of SAR and B_1-field within human head excited by MRI birdcage coils," in *Proc. IEEE Antennas Propag. Soc. Int. Symp.*, Montreal, QC, Canada, vol. 2, Aug. 1997, pp. 1210–1213.

[15] J. Jin and J. Chen, "On the SAR and field inhomogeneity of birdcage coils loaded with the human head," *Magn. Reson. Med.*, vol. 38, no. 6, pp. 953–963, 1997.

[16] T. S. Ibrahim, R. Lee, B. A. Baertlein, and P.-M.-L. Robitaille, "B1 field homogeneity and SAR calculations for the birdcage coil," *Phys. Med. Biol.*, vol. 46, no. 2, pp. 609–619, Feb. 2001.

[17] W. Liu, C. M. Collins, P. J. Delp, and M. B. Smith, "Effects of end-ring/shield configuration on homogeneity and signal-to-noise ratio in a birdcage-type coil loaded with a human head," *Magn. Reson. Med.*, vol. 51, no. 1, pp. 217–221, Jan. 2004.

[18] W. A. Anderson, "Electrical current shims for correcting magnetic fields," *Rev. Sci. Instrum.*, vol. 32, no. 3, pp. 241–250, 1961.

[19] A. L. Neves, L. Leroi, Z. Raolison, N. Cochinaire, T. Letertre, R. Abdeddaïm, S. Enoch, J. Wenger, J. Berthelot, A.-L. Adenot-Engelvin, N. Malléjac, F. Mauconduit, A. Vignaud, and P. Sabouroux, "Compressed perovskite aqueous mixtures near their phase transitions show very high permittivities: New prospects for high-field MRI dielectric shimming," *Magn. Reson. Med.*, vol. 79, no. 3, pp. 1753–1765, Mar. 2018.

[20] P. Ullmann, S. Junge, M. Wick, F. Seifert, W. Ruhm, and J. Hennig, "Experimental analysis of parallel excitation using dedicated coil setups and simultaneous RF transmission on multiple channels," *Magn. Reson. Med.*, vol. 54, no. 4, pp. 994–1001, 2005.

[21] J. T. Bushberg and J. M. Boone, *The Essential Physics of Medical Imaging*. Philadelphia, PA, USA: Lippincott Williams & Wilkins, 2011.

[22] G. Saleh, K. Solbach, and A. Rennings, "EBG structure to improve the B1 efficiency of stripline coil for 7 Tesla MRI," in *Proc. 6th Eur. Conf. Antennas Propag. (EUCAP)*, Prague, Czech Republic, Mar. 2012, pp. 1399–1401.

[23] Z. Chen, K. Solbach, D. Erni, and A. Rennings, "Improved B1 distribution of an MRI RF coil element using a high-impedance-surface shield," in *Proc. German Microw. Conf.*, Nuremberg, Germany, Mar. 2015, pp. 111–114.

[24] Z. Chen, K. Solbach, D. Erni, and A. Rennings, "Electromagnetic field analysis of a dipole coil element with surface impedance characterized shielding plate for 7-T MRI," *IEEE Trans. Microw. Theory Techn.*, vol. 64, no. 3, pp. 972–981, Mar. 2016.

[25] G. Saleh, K. Solbach, D. Erni, and A. Ashyap, "Tuning high impedance surfaces using coaxial cables for magnetic resonance imaging machines," *Int. J. RF Microw. Comput.-Aided Eng.*, vol. 28, no. 7, Sep. 2018, Art. no. e21477.

[26] K. Lezhennikova, C. Simovski, R. Abdeddaim, R. Balafendiev, and S. Glybovski, "Extending a birdcage coil for magnetic resonance imaging of a human head with an artificial magnetic shield," *Photon. Nanostruct. Fundamentals Appl.*, vol. 43, Feb. 2021, Art. no. 100890.

[27] Y. Soutome, H. Habara, Y. Bito, H. Takeuchi, T. Takahashi, and H. Ochi, "High-frequency coil unit and magnetic resonance imaging device," U.S. Patent 9 274 189, Mar. 1, 2016.

[28] C. Leeuwen, S. Glybovski, P. Luijten, C. van den Berg, and A. Raaijmakers, "Split-ring-resonator shield improves SAR efficiency and homogeneity of birdcage antenna," in *Proc. Int. Soc. Magn. Reson. Med.*, Montreal, QC, Canada, 2019, pp. 1–8.

[29] C. Leussler and C. Findeklee, "Z-segmented RF coil for MRI with gap and RF screen element," U.S. Patent 15 517 287, Oct. 26, 2017.

[30] L. Eberler, J. Nistler, and M. Vester, "MR antenna with compensation for variable distance to shield," U.S. Patent 9 829 549, Nov. 28, 2017.

[31] J. S. Tropp, D. K. Sodickson, and M. A. Ohliger, "Shielded TEM surface array for parallel imaging," U.S. Patent 7 015 695, Mar. 21, 2006.

[32] T. S. Ibrahim, R. Lee, B. A. Baertlein, A. M. Abduljalil, H. Zhu, and P.-M.-L. Robitaille, "Effect of RF coil excitation on field inhomogeneity at ultra high fields: A field optimized TEM resonator," *Magn. Reson. Imag.*, vol. 19, no. 10, pp. 1339–1347, Dec. 2001.

[33] J. Kennedy and R. Eberhart, "Particle swarm optimization," in *Proc. IEEE ICNN*, vol. 4, Nov./Dec. 1995, pp. 1942–1948.

[34] A. J. Poggio and E. K. Miller, *Computer Techniques for Electromagnetics*. New York, NY, USA: Pergamon Press, 1973.

[35] A. Guissard, "On the surface field integral equations," *IEEE Trans. Educ.*, vol. 46, no. 4, pp. 486–496, Nov. 2003.

[36] R. Harrington, *Time-Harmonic Electromagnetic Fields*. New York, NY, USA: McGraw-Hill, 1961.

[37] S. M. Rao, C.-C. Cha, R. L. Cravey, and D. L. Wilkes, "Electromagnetic scattering from arbitrary shaped conducting bodies coated with lossy materials of arbitrary thickness," *IEEE Trans. Antennas Propag.*, vol. 39, no. 5, pp. 627–631, May 1991.

[38] K. Umashankar, A. Taflove, and S. M. Rao, "Electromagnetic scattering by arbitrary shaped three-dimensional homogeneous lossy dielectric objects," *IEEE Trans. Antennas Propag.*, vol. AP-34, no. 6, pp. 758–766, Jun. 1986.

[39] R. S. Elliot, *Antenna Theory and Design*. Englewood Cliffs, NJ, USA: Prentice-Hall, 1981.

[40] J. I. Echeveste, D. Tihon, M. Dubois, R. Abdeddaim, S. Enoch, and C. Craeye, "Efficient and full-wave electromagnetic analysis of MRI antennas using the array scanning method," in *Proc. 12th Eur. Conf. Antennas Propag. (EuCAP)*, London, U.K., 2018.

[41] M. A. Carr, J. L. Volakis, and D. C. Ross, "Acceleration of free-space discrete body of revolution codes by exploiting circulant submatrices," *IEEE Trans. Antennas Propag.*, vol. 50, no. 9, pp. 1319–1322, Sep. 2002.

[42] Y. C. Kim, H. D. Kim, B.-J. Yun, and S. F. Ahmad, "A simple analytical solution for the designing of the birdcage RF coil used in NMR imaging applications," *Appl. Sci.*, vol. 10, no. 7, p. 2242, Mar. 2020.

[43] *CST Studio Suite*, Dassault Corp., Vélizy-Villacoublay, France, 2021.

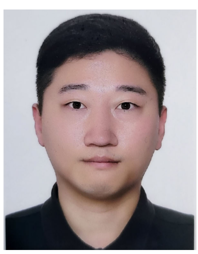

CHAN-SUN PARK received the B.S. and Ph.D. degrees in electrical and electronic engineering from Yonsei University, Seoul, South Korea, in 2012 and 2019, respectively. He is currently a Postdoctoral Researcher with the Institute of Information and Communication Technologies, Electronics and Applied Mathematics (ICTEAM), Université Catholique de Louvain (UCLouvain), Ottignies-Louvain-la-Neuve, Belgium. His current research interests include computational electromagnetics based on integral equations, static and dynamic multipole approach, and magnetic resonance imaging.

DENIS TIHON (Member, IEEE) received the M.Eng. degree in physical engineering and the Ph.D. degree in electrical engineering from the Université Catholique de Louvain (UCLouvain), Ottignies-Louvain-la-Neuve, Belgium, in 2013 and 2018, respectively.

From 2013 to 2019, he was a Teaching Assistant with UCLouvain and worked on the modeling of periodic absorbers illuminated by partially coherent fields. From 2017 to 2019, he participated in the M-Cube FET-OPEN European Project during which he worked on the simulation of magnetic resonance imaging (MRI) antennas. From 2019 to 2021, he worked on the modeling and measurement of partially coherent fields from luminescent sources with the Cavendish Laboratory, University of Cambridge, U.K., under a Marie Sklodowska-Curie Fellowship. Since 2021, he has been a Postdoctoral Researcher with UCLouvain, continuing his research on luminescent emitters. His current research interests include computational electromagnetism, the modeling of partially coherent fields, periodic and non-periodic absorbers, luminescent light sources, and reciprocity.

FARZAD JABBARIGARGARI was born in Gargar, Jolfa, Iran. He received the B.S. and M.S. degrees in electrical engineering from Urmia University, Urmia, Iran, in 2013 and 2016, respectively. He is currently pursuing the Ph.D. degree with the Université Catholique de Louvain, Ottignies-Louvain-la-Neuve, Belgium. His research interests include numerical electromagnetics and radio-frequency coils for magnetic resonance imaging.

REDHA ABDEDDAIM was born in Alger, Algeria, in 1979. He received the Ph.D. degree in physics from Université Paris Nanterre (formerly known as Paris X University), Paris, France, in 2007. He is currently an Assistant Professor with Aix-Marseille Université, Marseille, France. His current research interests include metamaterials, antennas, and magnetic resonance imaging (MRI) coils.

CHRISTOPHE CRAEYE (Senior Member, IEEE) was born in Belgium, in 1971. He received the master's degree in electrical engineering and the B.Phil. degree from the Université Catholique de Louvain (UCLouvain), Ottignies-Louvain-la-Neuve, Belgium, in 1994, and the Ph.D. degree in applied sciences from UCLouvain, in 1998. From 1994 to 1999, he was a Teaching Assistant with UCLouvain and carried out research on the radar signature of the sea surface perturbed by rain, in collaboration with NASA and the European Space Agency (ESA). From 1999 to 2001, he was a Postdoctoral Researcher with the Eindhoven University of Technology, Eindhoven, The Netherlands. He was with the University of Massachusetts, Amherst, MA, USA, in 1999. He was with the Netherlands Institute for Research in Astronomy, Dwingeloo, The Netherlands, in 2001. In 2002, he started an antenna research activity with UCLouvain, where he is currently a Professor. He was with the Astrophysics and Detectors Group, University of Cambridge, Cambridge, U.K., in 2011. His research was funded by the Region Wallonne, the European Commission, ESA, Fonds National de la Recherche Scientifique (FNRS), and UCLouvain. His current research interests include mutual coupling, finite antenna arrays, wideband antennas, small antennas, metamaterials, fast physical optics, and numerical methods for fields in periodic media, with applications to communication and sensing systems. He received the 2005–2008 Georges Vanderlinden Prize from the Belgian Royal Academy of Sciences, in 2009. He was an Associate Editor of the IEEE Transactions on Antennas and Propagation, from 2004 to 2010, and the IEEE Antennas and Wireless Propagation Letters, from 2011 to 2017.